Applied Acoustics 155 (2019) 97–110

Contents lists available at ScienceDirect

Applied Acoustics

journal homepage: www.elsevier.com/locate/apacoust

Investigation of a microphone height correction for long-range wind farm noise measurements

Kristy L. Hansen [a,*], Branko Zajamšek [a], Colin H. Hansen [b]

[a] College of Science and Engineering, Flinders University, Tonsley 5042, Australia
[b] School of Mechanical Engineering, University of Adelaide, Adelaide 5005, Australia

ARTICLE INFO

Article history:
Received 23 October 2018
Received in revised form 3 May 2019
Accepted 14 May 2019

ABSTRACT

In the measurement of wind farm noise, it is standard practice to mount outdoor microphones at a height of 1.5 m. On the other hand, measurements at this height can be affected by wind-induced noise, which has the potential to mask the noise of interest, particularly at low and infrasonic frequencies. Therefore, to minimise wind-induced noise, it is advantageous to measure on or below the ground, where the wind speed is close to zero. However, results from measurements taken at any height other than 1.5 m must be interpreted with caution, due to different interference effects between direct and ground-reflected waves at each location. This investigation explores the feasibility of using a prediction model based on Nord2000 algorithms to correct the 1/3-octave sound pressure level measured at ground level to obtain a representative value for a height of 1.5 m. The model takes into account phase changes due to the difference in travel-time for the direct and reflected rays and finite ground impedance, multiple source contributions and incoherence due to turbulence. The focus is on propagation distances greater than 2 km, where limited validation of existing propagation models has been attempted previously. Comparison is made between the model and measurement results obtained at four locations near a wind farm, where microphones were mounted at a height of 1.5 m and at ground level. A lack of agreement between measurements and the model indicates that the efficient and practical correction method considered here is not feasible for long-range wind farm measurements. Thus, it is recommended that wind farm noise is measured at both 1.5 m (for mid- to high-frequency noise) and at ground level (for low-frequency noise, which is more affected by wind).

1. Introduction

Wind farm noise contains a significant amount of low-frequency energy (less than 200 Hz) and it is predicted that the noise spectrum will shift further to lower frequencies as wind turbines inevitably increase in size [1]. The low-frequency components of wind farm noise can become dominant as the noise propagates away from a wind farm, due to atmospheric and ground absorption of the noise at mid- to high-frequencies. Moreover, noise in the mid- to high-frequency range is selectively attenuated by the walls and roof, resulting in an unbalanced spectrum inside a typical residence [2]. Since low-frequency noise has the potential to be annoying, particularly in the absence of mid- to high-frequency noise [3], its accurate characterisation is important and hence wind-induced noise must be minimised during noise level measurements.

A common technique for reducing wind-induced noise at the microphone is to use a large secondary wind screen in addition to the standard primary wind screen. The secondary wind screen provides a larger surface area over which the incoherent wind-induced noise is averaged [4] and the volume of air between the wind screen layers allows viscous dissipation of turbulence prior to it reaching the microphone [5]. In addition to using a secondary wind screen of practical size, the microphone can be placed as close as possible to the ground, where the atmospheric turbulent fluctuations and vortex shedding about the wind screen are minimal. Commonly used secondary wind screens are of hemispherical or spherical shape, where the former is used for measurement at ground level and the latter for measurements at a height of 1.5 m [6]. Data presented in the ANSI/ASA S1.18-2010 standard [7] indicate that measuring at ground level is advantageous if the signal of interest is dominated by low frequencies. This can be seen by comparing the overall C-weighted and G-weighted sound pressure levels (SPLs) measured at heights of 1.5 m and ground level, using a 300 mm wind screen and a wind screen designed according to the IEC 61400–11 Part 3 standard [8], respectively. At wind

* Corresponding author.
E-mail address: kristy.hansen@flinders.edu.au (K.L. Hansen).

https://doi.org/10.1016/j.apacoust.2019.05.015
0003-682X/

speeds above 3–4 m/s, the C-weighted and G-weighted levels are significantly lower when measurements are taken on the ground [7].

Wind farm noise can reach a given residence via a number of propagation paths, particularly when there are multiple wind turbines involved. The phase of incident sound waves depends on the distance between the turbine source and receiver, ground impedance and the number of ground reflections that have occurred during propagation. Depending on their relative phase, the direct and ground-reflected waves can interfere either in a constructive or destructive manner. Microphones that are mounted at various heights above the ground will be subject to variations in ray travel-time and ground reflection angles. Hence, it is expected that there will be frequency dependent variations in the SPL measured by these microphones. Ideally, a theoretical/engineering model would provide corrections that could be applied to the results of measurements made at heights other than 1.5 m.

The aim of this investigation is to apply existing theory to determine whether a practical engineering model can be used to correct 1/3-octave wind farm noise measured at ground level to obtain representative SPL values for a height of 1.5 m. The focus is on noise propagation from a wind farm to residences located more than 2 km from the nearest wind turbine. This scenario is highly relevant for measurements of wind farm noise, which are often taken at such large distances from the source, particularly in rural Australia. At present, available microphone height corrections are limited to distances of less than 1.6 km and do not take into account ground reflection effects and multi-source contributions (see Annex C in ANSI S12.9-7 [7]). In this investigation, long-term measurement data obtained at four different locations near an operating wind farm are analysed, where microphones were mounted at a height of 1.5 m and at ground level. The analysis is limited to conditions during which wind farm noise is expected to be dominant. The results are compared to a theoretical model that builds upon a more simplistic model previously described in Hansen et al. [9]. The model in this work takes into account phase changes due to the ray travel-time differences and finite ground impedance, multiple source contributions and incoherence due to turbulence. Ground-reflected waves that have undergone more than one reflection are not included in the theoretical analysis since only one reflection is predicted to occur for the sound rays originating from the wind turbines closest to the measurement locations.

2. Methodology

2.1. Measurement locations

Measurements of outdoor noise were carried out at four residences located within a few kilometres of the Waterloo wind farm, in South Australia. At the time of the measurements, the wind farm consisted of 37 wind turbines, each of rated power 3 MW and 80 m hub height. The wind farm is positioned along the top of a ridge and hence, the wind turbine hub height relative to the residences varies between 160 m and 215 m.

The four residences are referred to as measurement locations H1 to H4, and are indicated in Fig. 1. Further information, including measurement locations and measurement dates is given in Table 1. The GPS coordinates of H1 to H4 are also provided in this table, as this information is used to calculate the distance between each wind turbine and the residence of interest. The height difference in this table refers to the difference in height between the hub of the nearest wind turbine source and the ground level at the receiver, which were determined using Google Earth. The measurements were mainly carried out during the Autumn and Winter of 2013.

At all measurement locations, outdoor acoustic measurements were made using two microphones that were protected using a hemispherical or spherical type of wind screen. These wind screen designs are described in more detail in Hansen et al. [6]. At locations H1, H3 and H4, data were recorded using a National Instruments 9234, 24-bit data acquisition system with a sampling frequency of 10240 Hz and G.R.A.S. type 40 AZ 1/2 inch microphones with 20 CG G.R.A.S. pre-amplifiers. These microphones have a flat frequency response from 0.5 Hz to 20 kHz and a noise floor of 17 dBA. At location H2, Brüel and Kjær (B&K) LAN-XI data acquisition hardware was used with B&K Pulse software and the microphones were B&K type 4955 with a flat frequency response from 6 Hz to 20 kHz and a noise floor of 6.5 dBA. Microphones were typically placed at least 20 m from the residence and at least 10 m from surrounding vegetation to minimise façade reflections and wind-induced vegetation noise, respectively.

The wind speed near the microphones was measured at heights of 1.5 m and 10 m using Davis Vantage Vue and Vantage Pro weather stations, respectively. These weather stations have a wind speed accuracy in the range of ±0.4 m/s. Hub-height wind speed data were available from the wind farm operator for the measure-

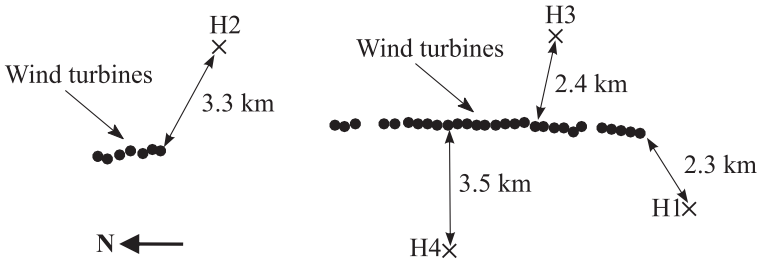

Fig. 1. Measurement locations in relation to the wind farm.

Table 1
Description of residence locations and measurement times.

Location	GPS coords	Measurement dates	Height difference	Microphone separation
H1	−34.0551 138.8904	8/5/13–13/5/13	160 m	6 m
H2	−33.9360 138.9409	24/7/13–9/8/13	151 m	12 m
H3	−34.0219 138.9416	14/5/13–20/5/13	169 m	3 m
H4	−33.9937 138.8798	19/2/13–21/2/13	215 m	2 m

ments at H1 and H3 and from a Fulcrum 3D SODAR for H1, H2 and H3. The SODAR was located on the same ridge-top as the wind turbines and the resolution of this device is ±0.01 m/s, according to the manufacturer. Hub-height wind speed data were not available for H4. Power output data for the Waterloo wind farm was obtained from the Australian Energy Market Operator website [10] in 5-min averages.

2.2. Data selection criteria

All acoustic and wind speed measurements were averaged over 10-min time intervals and data were selected for analysis based on three criteria: wind farm power output greater than 50% of its maximum; wind speed at 1.5 m height less than or equal to 1.5 m/s and residence located downwind (±45°) from the nearest wind turbine (according to hub height data). The specified wind direction from turbine to receiver is an approximation that was only accurate for the nearest turbine. However, as the wind farm layout is approximately linear in the North-South direction and most of the residences are located to the East and West of the wind turbines, the residences were usually downwind of the turbines that contributed significantly to the overall residence noise level. These criteria were imposed to ensure that wind farm noise was present in the measured signal and that wind-induced noise at the microphone was minimised. The number of 10-min-average measurements that met these criteria and the associated average wind farm power output are shown for each residence in Table 2. The absence of extraneous noise was verified through viewing the data in the time domain, observing the spectral characteristics of the measured signals and listening to the audio files.

2.3. Analysis of measurement data

The data that met the selection criteria outlined in Section 2.2 were averaged to investigate the applicability of a general correction for microphone height. An alternative approach could involve separating the data into hub-height wind speed bins; however, this was deemed unnecessary for two main reasons:

1. The variation in SPL that arises due to changes in hub-height wind speed, and hence power output and wind farm noise generation, is cancelled out when considering the SPL *difference* between simultaneous measurements made at heights of 1.5 m and 0 m.
2. Improved agreement between the measurements and model was not achieved when data were separated into wind speed bins of 1 m/s width.

These points are discussed in more detail in Section 3.1.

The average SPLs, $\overline{L}_p$, were determined by finding the logarithmic mean of the data that fulfilled the criteria described in Section 2.2, in each 1/3-octave band. The standard deviation, σ, for the n sound pressure level measurements, $L_{pj}(j = 1, n)$, that satisfied the selection criteria, was calculated using Eq. (1) [11].

Table 2
Number of data points that satisfied the selection criteria and the associated average power output.

Location	No. data points	Avg. Power Output
H1	59	64%
H2	29	58%
H3	50	60%
H4	15	64%

$$\sigma = \sqrt{\frac{\sum_{j=1}^{n}\left(L_{pj} - \overline{L}_p\right)^2}{n-1}} \tag{1}$$

The average SPL difference, $\Delta L_{p,avg}$, between measurements at heights of 1.5 m and ground level is a function of frequency and is calculated as follows [11]:

$$\Delta L_{p,avg}(f) = 10\log_{10}\left[\frac{1}{n}\sum_{j=1}^{n}\left(10^{\Delta L_{pj}(f)/10}\right)\right] \tag{2}$$

where $\Delta L_{pj}(f)$ is the level difference between the noise measured at a height of 1.5 m and at ground level for each measurement, j, with a total of n measurements at a given location.

The standard deviation, σ_Δ, in decibels, is obtained at each frequency using [11]:

$$\sigma_\Delta(f) = \left[\frac{1}{n-1}\sum_{j=1}^{n}\left(\Delta L_{pj}(f) - \Delta L_{p,avg}(f)\right)^2\right]^{1/2} \tag{3}$$

3. Model description

The model applied in this paper considers the noise contribution from all 37 wind turbines in the wind farm. Since the distance between the nearest wind turbine and each residence is greater than 2 km in all cases, a point source assumption has been adopted, which is expected to result in negligible error at such distances [12]. The wind turbine sources are also assumed to be incoherent. To model the difference in SPL at a height of 1.5 m and ground level, the phase difference between the direct and ground-reflected rays from each wind turbine is considered. For the microphone mounted on the ground, the ray travel-time difference between the direct and reflected waves is negligible and therefore the phase difference is caused by the ground reflection only. On the other hand, when determining the phase difference between direct and reflected waves for the microphone mounted at 1.5 m, both ray travel-time difference and ground reflection effects are important. Therefore, the SPL measured at a height of 1.5 m can be different to the one measured on the ground and the difference is frequency dependent.

The methodology used to determine the phase difference resulting from the variation in ray travel-times for the direct and ground-reflected rays will be discussed in Section 3.1. This is followed by a description of the technique used to determine the phase change due to ground reflection in Section 3.2. The phase information is then used to determine the predicted difference in phase, as a function of frequency, for the direct and ground-reflected sound rays arriving at the microphone mounted at ground level and the microphone mounted at a height of 1.5 m. The effect of atmospheric turbulence on the interference between the direct and ground-reflected rays is taken into account by incorporating a coherence coefficient into the model. The total SPL resulting from the partially coherent addition of the direct and ground-reflected waves is then determined for the ground-mounted microphone and for the microphone at a height of 1.5 m for each individual wind turbine contribution.

The total sound pressure at each microphone location due to all wind turbines is then found by adding the squared pressures resulting from each turbine, where the total sound pressure due to each turbine is normalised by the distance of the turbine from the receiver. The difference in dB between the total SPLs at the two microphones is then calculated as a function of frequency. This approach is based on the assumption that all turbines in the wind farm are radiating the same sound power at each frequency.

In the development of the practical, but approximate engineering model using circular ray paths, a number of assumptions and

approximations were necessary to minimise the amount and detail of the required input data. These are listed below:

1. For the propagation distances under consideration, the wind turbines may be modelled as incoherent point sources.
2. At any given point in time, all wind turbines radiate the same sound power at each frequency.
3. The vertical atmospheric sound speed profile is logarithmic.
4. The average ray height, h, is calculated using a two-parameter fit of h versus range.
5. For the propagation time calculations, the sound speed corresponding to the average ray height, h, is used for the entire ray path.
6. The ground flow resistivity, R_1, is 100 kPa s/m^2 at all residences.
7. A single ground reflection occurs between the source and receiver.
8. The extent of coherence between the direct and ground reflected rays is calculated using an atmospheric turbulence model as a basis.
9. The phase shift due to ground reflection is calculated using the spherical wave ground reflection coefficient as a basis.

The required input data for the approximate model are listed below:

1. Source-receiver distance for each wind turbine.
2. Source/receiver height above the ground.
3. Source height above the receiver.
4. Flow resistivity of the ground in the vicinity of the expected ground reflection location.
5. Wind velocity at hub height.

3.1. Phase difference due to ray travel-time

To calculate the length of both the direct and reflected ray paths, it is necessary to find the radius of curvature of the sound rays. This is dependent upon the vertical gradient of the speed of sound, which can be caused either by a wind gradient or by a temperature gradient, or by both [13]. A sound ray travelling at an angle, ψ_S above (or below) the line parallel to the ground plane will have a curved path with radius of curvature, R_c, at height, h, given by the following equation [14], where c is the speed of sound at height, h. When R_c is positive the sound rays are curved downward, towards the ground, and when R_c is negative, the sound rays are curved upward, away from the ground:

$$R_c = \frac{c}{\left[\frac{dc}{dh}\right]\cos\psi_S}. \tag{4}$$

For sound propagation in an atmosphere with small temperature and velocity gradients, and hence negligible refraction, it can be assumed that sound ray paths follow straight lines. To include the effects of moderate atmospheric refraction, it can be assumed that the sound speed follows a logarithmic profile. The associated sonic gradient is a function of height, h, above the ground. In this investigation, a representative, fixed value of h was chosen for the purpose of calculating a linearised wind gradient and corresponding radius of curvature of the sound ray, as will be discussed further in Section 3.1. The resulting sonic gradient is linear, allowing a circular ray path approximation, which makes the problem tractable. Alternatively, numerical ray tracing can be used for non-linear sound speed profiles using methods such as the one described in Chapter 3 of Ostashev and Wilson [15]. The disadvantage of this type of approach is that it requires significantly more computational time and can produce unstable and erroneous results in some cases [16]. Moreover, some difficulties can be encountered in the presence of varying topography between the source and receiver. Hence, the circular ray path assumption is a practical approach that is useful in engineering applications. The approximate models presented in this paper assume both straight ray propagation and curved ray propagation based on circular ray paths. Comparison is made to a numerical model that takes into account the non-linear sound speed profile by approximating the vertical sound speed variations using piecewise linear gradients and a vertical step size of 0.01 m. This model also includes a correction for the slope of the ground between the source and receiver. The comparison provides insight into the reasons behind observed differences between the approximate models and measured results.

The speed of sound, $c(h)$, at height, h, is a function of both the atmospheric horizontal wind speed profile and the atmospheric temperature profile. Assuming that the wind speed follows a logarithmic profile, the sound speed is expressed as follows [16]:

$$c(h) = B_m \log_e\left(\frac{h}{z_0}+1\right) + A_m h + c_0, \tag{5}$$

where c_0 is the speed of sound at height, $h = 0$, corresponding to the air temperature adjacent to the ground. Eq. (5) can be differentiated to obtain the sonic gradient:

$$\frac{dc}{dh} = A_m + \frac{B_m}{h+z_0}. \tag{6}$$

Substituting Eq. (6) into (4) gives the following expression for the radius of curvature of the sound ray:

$$\frac{1}{R_c} = \frac{1}{c}\left[A_m + \frac{B_m}{h+z_0}\right]\cos\psi_S. \tag{7}$$

Procedures to evaluate A_m and B_m are discussed below. Once these parameters have been evaluated, Eq. (7) can be used to find the radius of curvature of a ray at any height, h, above the ground. However, since the sound speed gradient, and hence radius of curvature of the sound ray, vary with h, it is necessary to assume a representative value of h for use in a practical engineering model. Therefore in this investigation, the height, h, was first selected as the height midway between the source and receiver heights above ground level for all wind turbines. This approach is similar to the Nord2000 model, which uses the average sound speed gradient between h_S and h_R to calculate R_c [16]. However, it was observed that the trajectory of the sound ray paths became higher with increasing source-receiver separation. Therefore, a linear function was used to define an estimated average ray height that increased as a function of distance. The function was adjusted until the best agreement was obtained between the model and measurements for H1. The resulting value of h was then used for H1 to H4. The value of h varied linearly between 47 m and 115 m over the distances from 2.3 km to 16.8 km. These distances represented the minimum and maximum separation between the wind turbines and H1 and the separation distances for all other residences and wind turbines were also within this range. Once the sound speed gradient was calculated for each wind turbine using Eq. (6), Eqs. (7), (10) and (11) were solved iteratively by increasing the value of ψ_S from $-\pi/2$ in increments of 0.001 radians until the value of ψ_S calculated using Eq. (10) was within 0.01 radians, which resulted in the sound ray intersecting the receiver.

The coefficient, A_m, is the vertical gradient of the speed of sound with height as a result of the atmospheric temperature profile and is given on p246 in Bies et al. [17] as:

$$A_m = \left[\frac{\partial c}{\partial h}\right]_T = \frac{dT}{dh}T^{-1/2}\frac{c_{00}}{2\sqrt{273}}, \tag{8}$$

where T is the temperature in Kelvin, c_{00} is the speed of sound at sea level, one atmosphere pressure and 0°C (331.3 m/s) and dT/dh is the

vertical temperature gradient (in Kelvin/m). Since temperature data as a function of height were not available, the value of dT/dh was assumed to lie within a realistic range (0 K/m to 0.01 K/m) for an atmosphere with moderate refraction [18]. The sensitivity of the model to the value of A_m was then investigated and it was found that the best fit between the model and measurements was obtained using $A_m = 0$.

The coefficient, B_m in Eq. (7) arises directly from the assumption of a logarithmic velocity profile. The value of B_m is found as follows [16]:

$$B_m = \frac{U_0}{\log_e\left(\frac{h_0}{z_0}+1\right)}, \tag{9}$$

where U_0 is the wind velocity at reference height, h_0, and z_0 is the roughness length. The roughness length, z_0, was set to 0.05, as the surrounding vegetation consisted of low crops [19]. The hub-height wind speed was the most representative value for U_0 from the available wind speed data. A typical plot of the wind speed measured by the SODAR in the height range between 50 m and 150 m above ground level (AGL) is shown in Fig. 2. The wind speed data presented in this plot were measured during the periods for which data were selected for H1. Three curve fits are shown and these are calculated using Eq. (9) and the minimum, mean and maximum velocity at hub height. The corresponding values of B_m are 1.16, 1.37 and 1.60. It can be seen that the logarithmic curve is a reasonable approximation of the velocity profile. Similar results were obtained for residences H2 and H3 and are thus not presented in this paper. In this investigation, the mean value of B_m was used in the calculations as this resulted in the best fit between the model and measurements. For comparison, the data were divided into wind speed bins of 1 m/s and the corresponding value of B_m was used in the model. It was found that the agreement between measurements and model was not improved using this approach and hence, the additional complexity of the analysis was not warranted.

The mean values of U_0 that were used in the analysis are listed in Table 3 along with the corresponding values of B_m. For H1 and H3, hub-height wind speed data from the wind farm operator were used and for H2, hub height SODAR data were used. Since the wind speed at hub height was not available for H4, the power output data were used to derive an approximate hub-height wind speed. This was done by finding the relationship between power output and hub-height wind speed based on data from the manufacturer [20]. The corresponding hub-height velocity could then be determined for each value of the power output.

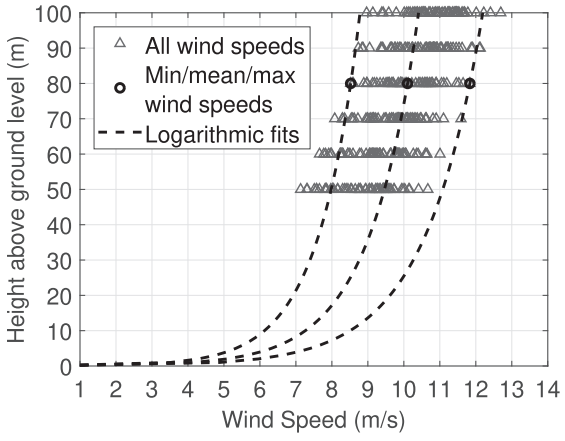

Fig. 2. Wind speed measured by the SODAR in the height range between 50 m and 150 m AGL and logarithmic fit using the hub height as the reference height in Eq. (9). Dashed lines show curve fits using the minimum, mean and maximum velocity at hub height.

Table 3
Values of B_m for each residence, corresponding to the mean hub-height wind speed, U_0, for measurements selected using the criteria in Section 2.2 for a surface roughness, z_0, of 0.05.

Location	U_0 (m/s)	B_m (m/s) from Eq. (9)
H1	9.8	1.33
H2	10.4	1.42
H3	11.8	1.59
H4	10.5	1.42

The angle, ψ_S, at which the sound ray leaves the source can be derived from inspection of Fig. 3 to obtain the following equation:

$$\psi_S = -\varphi + \arcsin\left(\frac{d}{2R_c\cos\varphi}\right), \tag{10}$$

where

$$\varphi = \arctan\left(\frac{h_S - h_R}{d}\right), \tag{11}$$

where h_S and h_R are the source and receiver heights, respectively. Note that the source height, h_S, is equal to the sum of the ridge height and hub height for all geometrical calculations and it is equal to the hub height above the ground immediately below the turbine for determining atmospheric parameters.

The angle, ψ_R, at which the sound ray arrives at the receiver can also be derived from inspection of Fig. 3 and is given by:

$$\psi_R = \arcsin\left(\frac{d - d_o}{R_c}\right), \tag{12}$$

where $d_o = R_c \sin\psi_S$.

These angles are used to determine the included angle, θ, for the curved path between the source, S and receiver, R, which is given by $\theta = \psi_S + \psi_R$. The distance, r, traveled by a direct ray to the receiver over an arc of a circle of radius, R_c, with an included angle of θ radians is given by $r = R_c\theta$.

The travel distance for the reflected ray is calculated using the same method as for the direct ray described above. When undertaking calculations for the reflected ray path between the source and reflection point, the receiver height is set to zero. For the reflected ray path between the reflection point and the receiver, the source height is set to zero. The reflection point is determined iteratively by selecting an initial point halfway between the source and receiver and shifting this point towards the receiver in increments of 0.1 m until the angle of incidence is equal to the angle of reflection, to an accuracy of 0.01 radians. Here, the angle of incidence refers to the angle ψ_R associated with the ray that travels from the source to the ground reflection point, which is calculated using Eq. (12). The angle of reflection is the angle ψ_S calculated by Eq. (10) for the ray that travels between the ground reflection point and receiver. For consistency, the approximate average ray height, h, was kept constant to calculate the ray path before and after the ground reflection. The total ray travel-time is the sum of the travel times between the source and reflection point and between the reflection point and the receiver.

To determine the validity of the simplification of assuming that only one ground reflection occurs, it is possible to determine the approximate number of rays, N_{rays}, that arrive at the receiver including the direct ray and rays that have only experienced a single ground reflection. The contribution from additional rays is ignored for $N_{rays} < 4$, as these rays have one or no reflections and have already been included [16]. The approximate number of rays, N_{rays}, that are possible between the source and receiver is given by Plovsing [16]:

$$N_{rays} = \frac{4d}{h_S}\sqrt{\frac{B_m}{2\pi c_0}}. \tag{13}$$

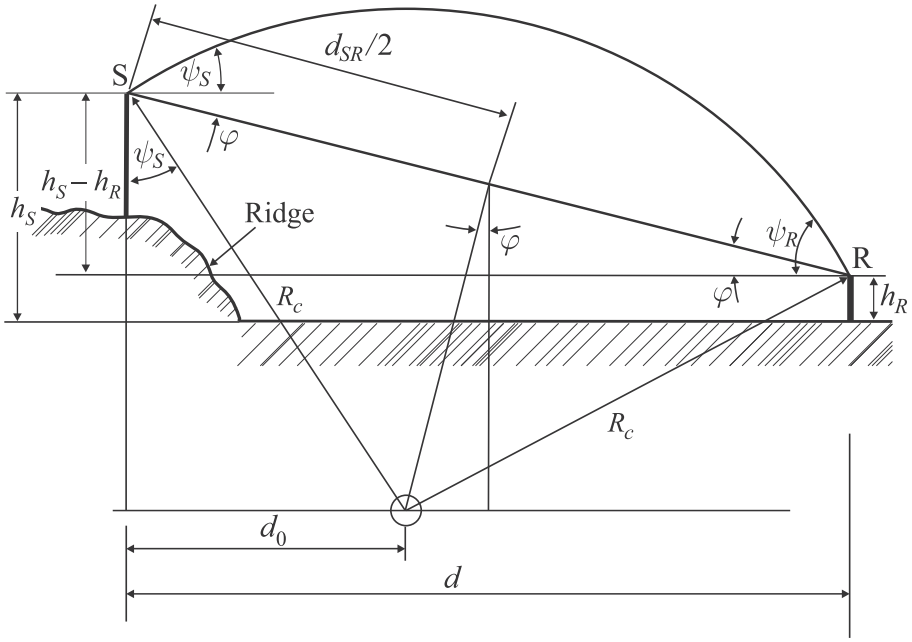

Fig. 3. Geometry for calculating the radius of curvature of a sound ray originating at source, S, and arriving at receiver, R, for a source higher than the receiver and for the maximum ray height between the source and receiver [17].

It was found that $N < 4$ for the nearest 18 wind turbines, at least for all cases considered in this analysis and this was also verified using the model, which gave a single reflection point close to the receiver. Thus, the assumption of a single ground reflection is reasonable.

In this investigation, a more simplified approach to determining the ray travel-time difference between the direct and reflected rays is also considered. This approach assumes that the sound speed gradient has a value close to zero, resulting in straight-ray propagation. While such an assumption is valid for short-range propagation and low source and receiver heights, it can result in errors for long-range propagation and high wind turbine sources such as those considered in this analysis. However, since the aim of this investigation was to develop a practical and efficient model and the ANSI S12.9-7 standard [7] makes this assumption, the method was investigated. Accordingly, the direct and reflected sound ray paths shown in Fig. 4, r and $r_S + r_R$, respectively, for the microphones mounted at heights of 1.5 m and ground level can be determined as follows:

$$r = \left[(h_S - h_R)^2 + d^2\right]^{1/2} \tag{14}$$

and

$$r_S + r_R = \left[(h_S + h_R)^2 + d^2\right]^{1/2}. \tag{15}$$

3.2. Phase difference due to reflection

When sound rays reflect at a plane interface between two media, they undergo a phase change, which is dependent on the properties of the media and the frequency of sound. According to Attenborough [21], when the angle, θ, in Fig. 4 is greater than 85°, the curvature of the wave front striking the ground must be

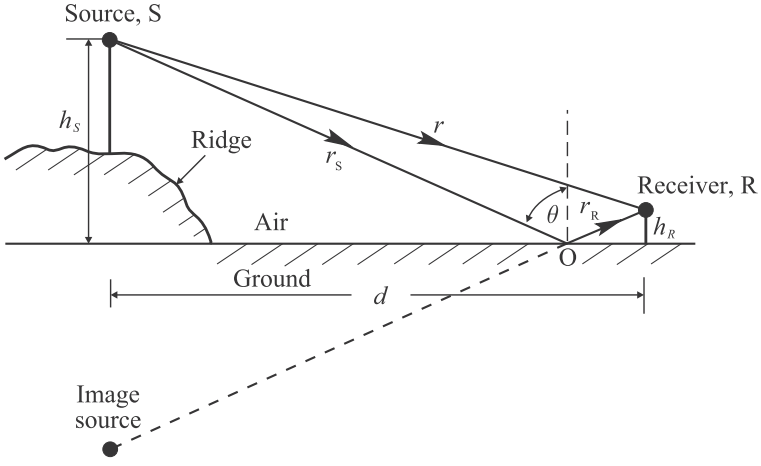

Fig. 4. Schematic showing the path of the direct and reflected wave, where the radius of curvature of sound rays is infinitely large.

taken into account by using a complex spherical wave coefficient. The complex amplitude reflection coefficient, Q, of a spherical wave incident upon a reflecting surface may be written as follows: [22]

$$Q = R_p + (1 - R_p)[BG(w)] = |Q|^{j\alpha_s}, \tag{16}$$

where the phase of the reflected wave relative to the incident wave is $\alpha_s = \tan^{-1}[\mathrm{Im}\{Q\}/\mathrm{Re}\{Q\}]$, and R_p is the plane wave reflection coefficient.

For realistic ground surfaces and $\theta \approx \pi/2$, it can be assumed that $B \approx 1$ and this approximation is made in Taherzadeh and Attenborough [23] and the ANSI/ASA S1.18-2010 standard [11]. A more general definition of B can be found in Eq. (41) in [22] and Eqs. (5.24) to (5.29) in [17]. In this investigation, Q was calculated in two ways: by using the assumption that $B \approx 1$ and also by using the more general equations. It was found that the final calculated SPL difference between microphone heights of 1.5 m and ground level differed by less than 0.1 dB for the two different values of B. Therefore, even though θ was much less than $\pi/2$ due to refraction effects, it was reasonable to assume that $B \approx 1$.

The argument, w, of $G(w)$ in Eq. (16), is referred to as the numerical distance and is calculated using the equation given in Attenborough [22]:

$$w = \frac{1}{2}(1 + \mathrm{j})[k(r_S + r_R)]^{1/2}\left(\cos\theta + \frac{\rho c}{Z_m}\right), \tag{17}$$

where $k = \omega/c$ is the wavenumber, c is the speed of sound in air and ρ is the density of air. The term, $G(w)$, in Eq. (16) is defined as:

$$G(w) = 1 + \mathrm{j}\sqrt{\pi} w g(w), \tag{18}$$

where

$$g(w) = \mathrm{e}^{-w^2}\,\mathrm{erfc}(-\mathrm{j}w), \tag{19}$$

where $g(w)$ is the scaled complementary error function, erfc() is the complementary error function [24], and w, is a complex number, given by Eq. (17). The scaled complementary error function, $g(w)$, can be calculated using Eqs. (5.34) to (5.42) in [17], corrected according to the errata available online atwww.causalsystems.com. Note that in this paper, equations for sound pressure use positive time dependence $\mathrm{e}^{j\omega t}$.

The plane wave reflection coefficient, R_p was calculated using Eq. (20), which is applicable for a locally reacting surface. Using Eq. (5.15) in [17], which is the more general form of the equation used to calculate R_p, resulted in less than 0.1 dB difference in the final calculated SPL difference between microphone heights of 1.5 m and ground level.

$$R_p = \frac{Z_m \cos\theta - \rho c}{Z_m \cos\theta + \rho c}. \tag{20}$$

The characteristic impedance of a porous material, in this case the ground, can be calculated using the Delaney and Bazley model [26]:

$$Z_m = \rho c\left[1 + 0.0571X^{-0.754} - \mathrm{j}0.087X^{-0.732}\right], \tag{21}$$

where the quantity, X, is defined as

$$X = \rho f/R_1, \tag{22}$$

where R_1 is the flow resistivity in the region where the ground reflection is expected to take place and f is the frequency of sound. A flow resistivity of 100 kPa s/m^2 was chosen in the analysis as this corresponds to the appropriate value for rough grassland and pasture [27], which was characteristic of the ground near the measurement microphones.

The plane wave reflection coefficient, R_p, can also be used in place of the spherical wave reflection coefficient, Q, when the angle, θ, in Fig. 4 is less than 85° [21]. Using the model described in Section 3.1 with refraction of sound rays taken into account, it was found that θ was in fact less than 85° for all cases and hence the plane wave reflection coefficient was a sufficient approximation in this investigation. While θ was found to be slightly higher than 85° when assuming straight ray propagation, particularly for propagation between the furthest wind turbines and the residences, use of R_p instead of Q resulted in less than 0.1 dB difference in the final calculated SPL difference between microphone heights of 1.5 m and ground level.

3.3. Total phase difference

The phase difference between direct and reflected waves for the microphone mounted at ground level arises from the reflection effects that were discussed in Section 3.2. For the microphone mounted at 1.5 m, both the ray travel-time difference between the direct and ground-reflected rays, discussed in Section 3.1, and the ground reflection effects need to be considered in the analysis. Fig. 4 illustrates the path of the direct wave and one reflected wave for the microphone mounted at a height of 1.5 m. The angles marked in this figure refer to the reflected wave. The figure shows straight ray propagation for simplicity but the parameter definitions are also relevant for refracted rays.

The pressure field, p, at each microphone due to a point source at height h_S above the plane boundary between two media (e.g. air and ground, see Fig. 4) is given by the Weyl-Van der Pol equation, which can be expressed in the form [28]:

$$p = P_d + P_r = A_0\frac{\mathrm{e}^{-\mathrm{j}kc_h\tau}10^{-\frac{(\alpha_a r)}{20}}}{r} + A_0\frac{\mathrm{e}^{-\mathrm{j}kc_h(\tau_S+\tau_R)}10^{-\frac{(\alpha_a(r_S+r_R))}{20}}}{(r_S + r_R)}Q, \tag{23}$$

where the pressure field, p, consists of contributions from the acoustic pressure due to the direct and reflected rays, which are denoted p_d and p_r, respectively. The parameters r and $r_S + r_R$ refer to the lengths of the direct and ground-reflected ray paths respectively, between the source and the microphone mounted at a height of 1.5 m, as shown in Fig. 4. The corresponding ray travel times are $\tau = r/c_h$ and $\tau_S + \tau_R = (r_S + r_R)/c_h$. The parameter c_h is the speed of sound at the approximate average ray height, h, described in Section 3.1. Also, Q is the spherical wave reflection coefficient defined in Eq. (16), which can be replaced by the plane wave reflection coefficient, R_p, defined in Eq. (20), when the grazing angle $(\pi/2 - \theta)$ is greater than 5°, as in this study. For the ground mounted microphone, there is negligible difference between the values of r and $r_S + r_R$, as well as the corresponding ray travel times, τ and $\tau_S + \tau_R$. The parameter, A_0 represents the amplitude of the pressure wave and α_a is the air absorption in dB/m, which is determined using the procedure described in ANSI-S1.26 [29]. While A_0 varies as a function of distance (i.e. depending on which wind turbine source is analysed), it is assumed that A_0 is the same for the direct and ground-reflected rays from each wind turbine at both mounting heights. This assumption does not affect the results since the direct ray paths to the two microphones are almost identical and hence the SPL difference due to different ray path distances is much less than the measurement precision. It is also emphasised that the *relative* phase between the direct and ground-reflected rays at *each* microphone is the parameter of interest that determines the difference in SPL between the two microphones.

Eq. (23) is derived based on the assumption that the direct and ground-reflected rays are fully coherent. However this is not necessarily the case, particularly at relatively high frequencies, where atmospheric turbulence reduces the coherence. This reduction in coherence is taken into account using a coefficient of coherence

due to turbulence, F_t, and the associated calculations are outlined in Section 3.4. The sound pressure, p_t, with turbulence effects included, arriving at the microphone locations from each wind turbine is given by Eq. (5.229) in Bies et al. [17]:

$$|P_t|^2 = |P_d|^2 \left[\left| 1 + F_t \frac{P_r}{P_d} \right|^2 + (1 - F_t^2) \left| \frac{P_r}{P_d} \right|^2 \right]. \tag{24}$$

The pressure squared contributions from all 37 wind turbines are then summed together for the receiver heights of 0 m and 1.5 m, respectively, giving $p^2{}_{\mathrm{tot,1.5m}}$ and $p^2{}_{\mathrm{tot,0m}}$. The log to the base 10 of the ratio of the resulting quantities is the SPL difference, ΔL_p between the two receiver heights. Thus:

$$\Delta L_p = 10 \log_{10} \left(\frac{p^2_{\mathrm{tot,1.5m}}}{p^2_{\mathrm{tot,0m}}} \right). \tag{25}$$

The quantities in Eq. (23) are calculated based on a frequency resolution of 1 Hz. Since the 1/3-octave SPL difference is the quantity of interest, the pressure squared contributions at all frequencies within a given 1/3-octave band are summed together separately for each microphone prior to implementing Eq. (25).

3.4. Coherence coefficient due to turbulence

The coherence coefficient due to turbulence is given by [30]:

$$F_t = \begin{cases} \mathrm{e}^X & X \geqslant -1 \\ (2 + X)\mathrm{e}^{-1} & -2 < X < -1 \\ 0 & X \leqslant -2 \end{cases} \tag{26}$$

where

$$X = -5.3888 \gamma_T \left(\frac{f}{\bar{c}} \right)^2 q^{5/3} d, \tag{27}$$

where the constant '5.3888' is as provided by Plovsing [25].

$$\gamma_T = \frac{C_T^2}{\bar{T} + 273.15} + \frac{22 C_v^2}{3 \bar{c}^2}, \tag{28}$$

where $\bar{T}$ is the average temperature over the sound propagation path, $\bar{c}$ is the average speed of sound corresponding to the average temperature, d is the horizontal distance between source and receiver, C_T^2 is the turbulence strength due to temperature effects (temperature turbulence structure parameter), C_v^2 is the turbulence strength due to wind effects (velocity turbulence structure parameter). The quantity, q, is half the mean separation of the direct and reflected ray paths and is defined as:

$$q = \frac{h_S h_R}{h_S + h_R}, \tag{29}$$

where h_S and h_R are the source and receiver heights above the ground.

The values of C_T^2 and C_v^2 are calculated according to Eq. (6.36) in Ostashev and Wilson [15]. It was assumed that the wind conditions were moderate and the atmospheric conditions weakly stable, such that u_* and Q_H were 0.3 and $-20 \mathrm{W/m^2}$, respectively. The values of C_T^2 and C_v^2 were calculated as 0.001 and 0.03, respectively. The mean temperature, $\bar{T}$, was obtained from the SODAR and corresponded to the temperature at ground level on the ridge. The corresponding value of γ_T was 5×10^{-6}, which is consistent with 'moderate turbulence' according to Salomons et al. [31].

4. Model validation

4.1. ANSI-S12.9-7 comparison

In the first step of the validation process, results were compared to tabulated values of the microphone height correction presented in Annex C of ANSI S12.9-7 [7]. This correction is based on the assumptions of straight ray propagation, single-source contribution, single reflection and negligible phase change on reflection. Hence, the SPL difference, ΔL_p, between the two receiver heights arises due to the coherent addition of the direct and ground-reflected rays at each receiver position. For the microphone mounted at 1.5 m, there is a phase difference of $k\Delta$ between the direct and ground-reflected rays due to the associated path-length difference, Δ. There is no phase difference for the ground-mounted microphone. Agreement between the results was generally within 0.5 dB and peaks and troughs occurred at the same frequencies as shown in Fig. 5.

4.2. ANSI-S1.18-2010 comparison

In the next step of the validation process, the phase change due to ground reflection effects was incorporated into the model. The relevant equations are given in Section 3.2 and Annex D of the ANSI/ASA S1.18-2010 standard [11]. The standard provides template curves A and B and these were used to check that the model was correct for two sets of microphone heights and flow resistivity

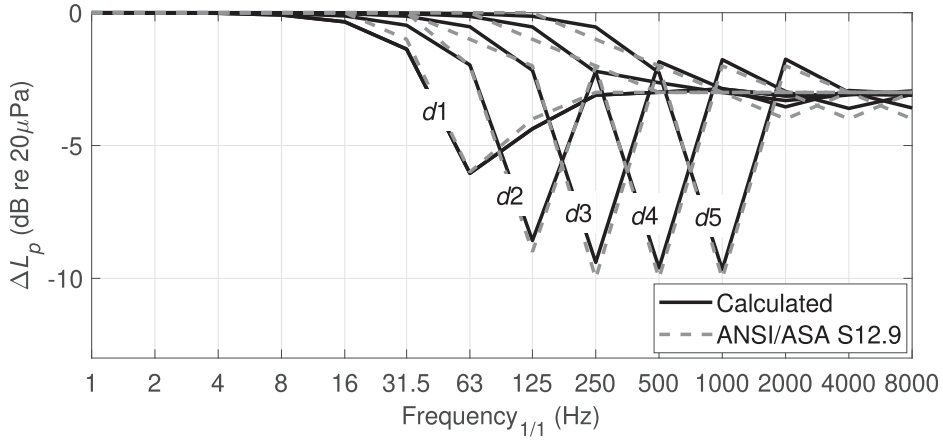

Fig. 5. Comparison between tabulated data in Annex C of ANSI S12.9-7 [7] and calculations based on assumptions of straight ray propagation, single-source contribution, single reflection and negligible phase change on reflection. The corrections are to convert microphone data measured at ground level to data corresponding to a height of 1.5 m. Calculations are based on a source height of $h_S = 80$ m and source-receiver separation distances of d_1–d_5 of 100 m, 200 m, 400 m, 800 m and 1600 m.

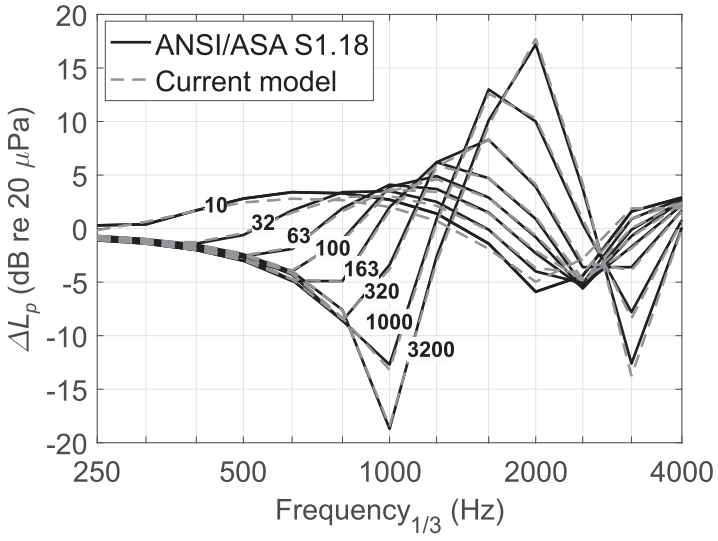

Fig. 6. Comparison between template curve A in ANSI S1.18-2010 [11] and the current model for flow resistivities between 10 and 3200 kPa s/m^2.

values ranging from 10 to 3200 kPa s/m^2. The results of comparison with template curve A are shown in Fig. 6 and indicate that the model behaves as expected. The geometry associated with template curve A is as follows: $h_S = 0.325\text{m}, h_R, t = 0.46\text{m}, h_R$, $b = 0.23\text{m}, d = 1.75\text{m}$, where $h_{R,t}$ and $h_{R,b}$ are the heights of the upper and lower microphones, respectively. The horizontal separation between microphones is d.

5. Results

5.1. Measurement results

Fig. 7 shows a comparison between the average SPLs, in 1/3-octave bands, measured using microphones mounted at heights of 0 m and 1.5 m above ground level, at locations H1 to H4.

The difference between the results for different microphone heights and wind screens in the frequency range between 3 Hz and 63 Hz is shown to be insignificant in Fig. 7. This is due to the relatively large wavelengths at these frequencies and the small ray travel-time differences between the direct and reflected waves, which results in a small phase difference and hence similar SPLs at both heights. Also, SPL differences due to wind-induced noise are negligible in this frequency range due to the fact that all data were measured during wind speeds $\leqslant$1.5 m/s. The difference in SPL reaches a maximum between 200 and 315 Hz. This maximum is observed at all residences and is due to a combination of the phase change in the reflected wave governed by the ground impedance (ground impedance is assumed to be similar at all residences) and the phase difference between the direct and ground-reflected rays. Between 315 and 1000 Hz, the difference between the results obtained at different heights decreases. Below 3 Hz, the SPL measured at the ground is lower than that measured at 1.5 m, as expected due to the influence of wind-induced noise. Thus, it can be seen that even at wind speeds $\leqslant$1.5 m/s, wind-induced noise can increase the measured SPL by more than 5 dB at these infrasonic frequencies.

5.2. Modelling results

5.2.1. Ray paths

The circular ray paths from each wind turbine source to the receiver at H1 are plotted in Fig. 8. Each ray path is drawn on a two-dimensional plane that is constructed based on the shortest path between the source and receiver. The rays from the nearest and furthest wind turbines are shown in dark and light colours, respectively. The turbines are shown using black lines and the height of their base corresponds to the ridge height relative to the residence at that point. The figure insert shows the direct and reflected rays for the nearest wind turbine. The reflected rays are not visible on the main plot due to the relatively large source height and source-receiver separation distance compared to the receiver height.

The corresponding plot for straight ray propagation is not shown here but the main differences are that the rays leave below the horizontal and the angle of incidence/reflection of the rays at the ground are smaller.

The ray paths for the closest five wind turbine sources to H1 are shown in Fig. 9 for the circular-ray model presented in this paper and the numerical model that accounts for the non-linear sound speed profile. The results obtained using the value of h that provided the best match between the circular-ray model and measurements are shown in Fig. 9a) and the results obtained using the average ray height from the numerical model are shown in Fig. 9(b). Note that the average ray height for the numerical model is calculated by averaging the segment heights, taking into account the relative lengths of each segment and also including the slope of the ground between the source and receiver. It can be seen that although the ray paths for the circular-ray and numerical models are in better agreement in Fig. 9(b), the ground reflection angle shows better agreement between the two models in Fig. 9(a). The implications of these results will be discussed in more detail in Section 6. Further details about the average ray heights used in the circular-ray model and calculated using the numerical model are provided in Table 4. This table also provides information on the ray travel times for the direct and reflected rays to the receiver height of 1.5 m for both the circular-ray model and the numerical model.

5.2.2. SPL difference

Fig. 10 shows the measured and predicted differences between the SPL, ΔL_p, at a height of 1.5 m and at ground level for all residences, considering all 37 wind turbines in the analysis. The grey dotted curve in each graph represents ΔL_p for the ANSI S12.9-7 model [7], which considers the path-length difference only. The grey dash-dot curve corresponds to ΔL_p for the straight ray model, which considers the path-length difference, reflection effects and incoherence due to turbulence. The black dashed curve is calculated based on ΔL_p for the circular-ray model and includes

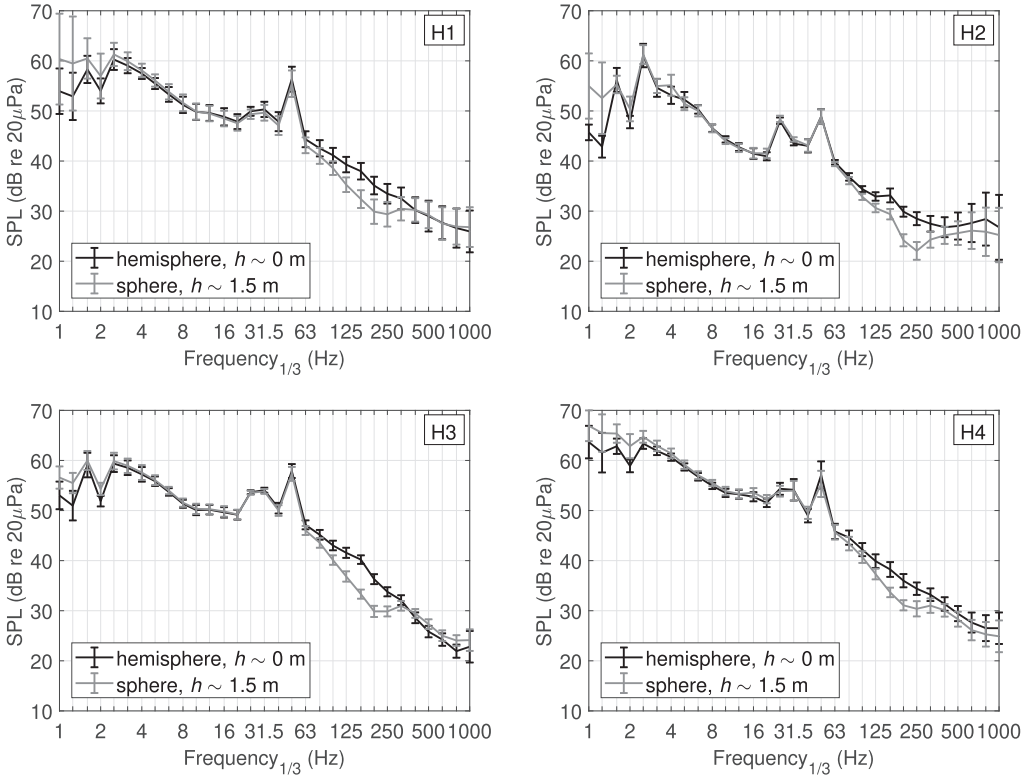

Fig. 7. 1/3-Octave band average measured SPLs, where the terms 'sphere' and 'hemisphere' refer to the secondary wind screens that were used to protect the microphones from wind-induced noise. The average SPL includes data that met the selection criteria presented in Section 2.2.

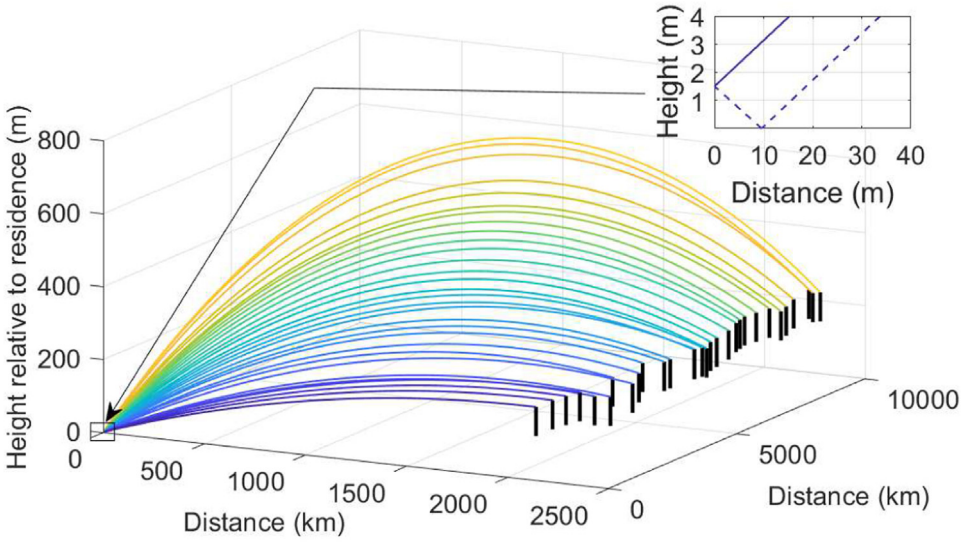

Fig. 8. Ray paths in the downwind direction, from the nearest 30 wind turbine sources to the receiver at H1, plotted in 3D. The rays from the nearest and furthest turbines are shown in dark and light colours, respectively and the wind turbines are shown as black lines. The source height is the sum of the ridge height at each turbine and the hub height of 80 m and the turbines are shown with their actual hub height of 80 m. Insert: Direct (solid blue line) and reflected (dashed blue line) rays from the nearest wind turbine. (For interpretation of the references to colour in this figure legend, the reader is referred to the web version of this article.)

reflection effects and incoherence due to turbulence. The predicted attenuation due to atmospheric absorption has been included in all models.

Both the measurements and models predict that the difference in SPL at frequencies below 80 Hz is expected to be less than 1.5 dB. The reason for this is that the ray travel-time difference and ground reflection have a small effect on the phase difference due to the large wavelengths of sound at these frequencies. All models predict that destructive interference occurs at the microphone mounted at 1.5 m and this agrees with the measurement results. The ANSI S12.9-7 model [7] demonstrates the worst performance, indicating that ground impedance effects and incoherence due to turbulence cannot be ignored in the analysis. The straight-ray model provides a reasonable estimate of the frequency at which the plot minimum occurs, however the magnitude is significantly underestimated. The circular-ray model provides the best

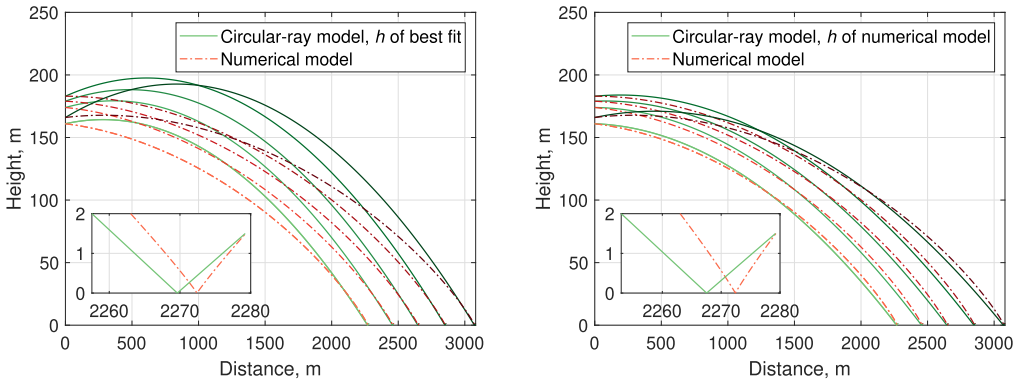

Fig. 9. Ray paths for the closest five wind turbine sources to H1, where the results of the circular-ray and numerical models are plotted using green and red dot-dash lines, respectively. The figure insert shows the ground-reflection for the closest receiver. The average ray height, h, is based on (a) best match with measurements and (b) calculated value from numerical model. (For interpretation of the references to colour in this figure legend, the reader is referred to the web version of this article.)

Table 4
Comparison between direct and reflected ray travel times for a receiver with a height of 1.5 m and average ray height for the circular-ray (approx.) and numerical models.

Turbine number	Travel time (s)				Average ray height	
	Direct ray		Reflected ray		Reached by direct ray (m)	
	Approx.	Numerical	Approx.	Numerical	Approx.	Numerical
1	6.4974	6.4776	6.4987	6.4796	47	64
2	7.0298	7.0056	7.0311	7.0075	48	66
3	7.5721	7.5440	7.5735	7.5459	49	68
4	8.1512	8.1189	8.1527	8.1207	50	70
5	8.7796	8.7443	8.7811	8.7471	51	73
6	9.4362	9.3975	9.4377	9.3990	52	76
7	10.7688	10.7156	10.7706	10.7177	54	81
8	11.1216	11.0656	11.1235	11.0666	55	82
9	11.8869	11.8215	11.8890	11.8229	56	85
10	12.5656	12.4903	12.5679	12.4927	57	88
11	13.3614	13.2781	13.3637	13.2796	58	92
12	14.0237	13.9328	14.0262	13.9344	59	95
13	14.8421	14.7384	14.8448	14.7396	61	98
14	15.4968	15.3862	15.4996	15.3886	62	101
15	16.2305	16.1104	16.2334	16.1128	63	104
16	16.9506	16.8231	16.9537	16.8253	64	108
17	17.6933	17.5540	17.6966	17.5561	65	111
18	18.3197	18.1711	18.3231	18.1730	66	114
19	19.0930	18.9318	19.0966	18.9328	68	117
20	19.8602	19.6849	19.8640	19.6873	69	120
21	20.5859	20.3998	20.5898	20.4014	70	124
22	21.3400	21.1423	21.3440	21.1437	71	127
23	22.1295	21.9183	22.1338	21.9201	73	131
24	22.9271	22.7018	22.9316	22.7039	74	135
25	23.7090	23.4733	23.7136	23.4749	75	139
26	24.7489	24.4954	24.7537	24.4974	77	144
27	25.5541	25.2844	25.5591	25.2864	78	148
28	27.8271	27.5182	27.8326	27.5198	82	160
29	28.6504	28.3266	28.6560	28.3286	83	165
30	29.4162	29.0808	29.4219	29.0829	85	170
31	43.0881	42.4755	43.0963	42.4777	107	250
32	43.8551	43.2286	43.8636	43.2305	108	257
33	44.5538	43.9100	44.5624	43.9119	109	259
34	45.5532	44.8876	45.5617	44.8894	111	266
35	46.4491	45.7622	46.4581	45.7642	112	270
36	47.3700	46.6619	47.3791	46.6640	114	275
37	48.1585	47.4325	48.1674	47.4345	115	280

performance, particularly for H1 and H3, where agreement between the measurements and model is within 1 dB up to 500 Hz. For H2, the frequency and magnitude of the plot minimum are underestimated and for H4 the frequency is underestimated and the magnitude is overestimated. According to the results presented here, the model could differ by up to 4 dB from measurements at the frequency where maximum destructive interference occurs. Although it is possible to 'tune' the model to achieve better agreement with measurements for H2 and H4, by adjusting the value of h used in Eq. (7), this is not a feasible approach in practice.

6. Discussion

The circular-ray model yielded excellent results for two cases presented in this study (H1 and H3) but for the other two cases

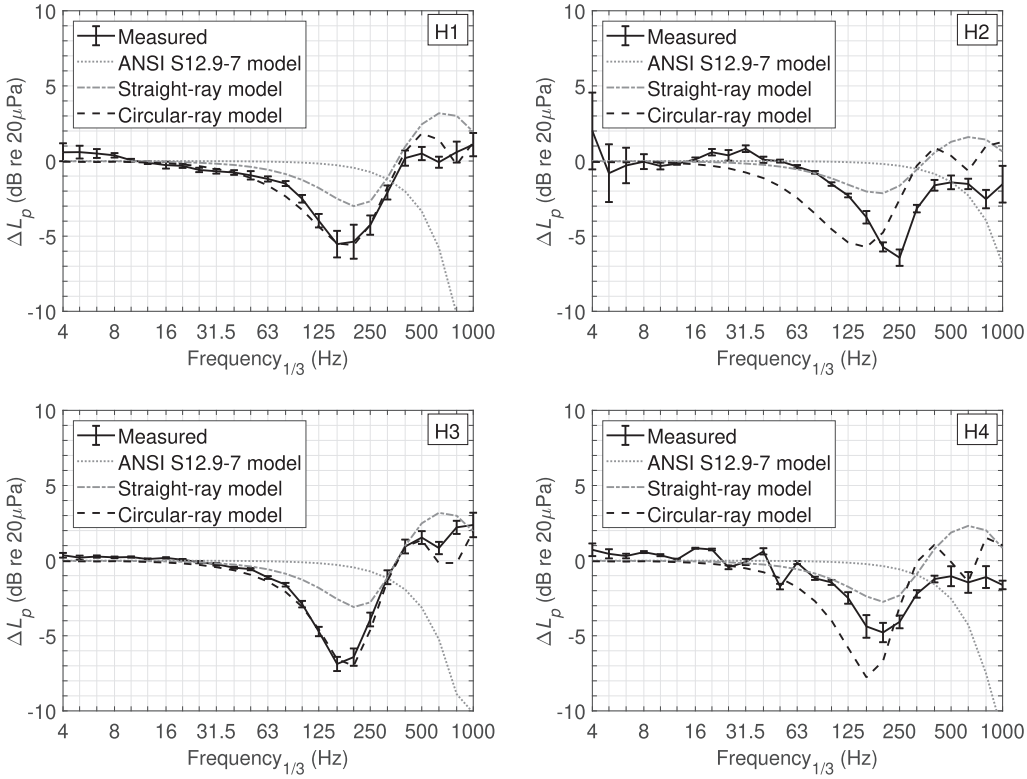

Fig. 10. Predicted and measured differences between the SPLs measured at a height of 1.5 m and the SPLs measured at ground level at locations H1 to H4. Predictions include noise contributions from all 37 wind turbines. The flow resistivity, R_1, used in the predictions was 100 kPa s/m^2 for all residences.

(H2 and H4), the results were marginally acceptable. This suggests that the approximate ray height, h, that provided the best fit between measurements and model for H1 was also representative for receivers located a similar distance from the wind farm, such as H3. However, for greater source-receiver separation distances, the value of h needed to be larger to obtain reasonable agreement with measurements. Therefore, the largest concern for the use of the circular-ray model is choosing the most representative value of the approximate ray height, h, to evaluate the linearised sonic gradient.

Comparison was made between the circular-ray model and a numerical model that took into account the non-linear sound speed profile. It was shown that when using the value of h that resulted in the best fit between measurements and the circular-ray model, the rays travelled to an unrealistic height. This increased both the path lengths and travel times of the rays. On the other hand, the ground-reflection angle was similar for the circular-ray and numerical models. When the average ray height, h, determined from the numerical model was used in the circular-ray model, the ray trajectories were more realistic but the ground-reflection angles were too small. The inability of the circular-ray model to achieve accurate ray paths and ground-reflection angles simultaneously is a consequence of the circular ray approximation. The better agreement obtained using the 'best fit' value of h for H1 and H3, indicates that for residences located relatively close to the nearest wind turbines, it was more important to model the ground reflection angles accurately than the ray travel times. For these cases, the difference in travel times between the direct and reflected rays from the closest wind turbines, which contribute most to the SPL at the receiver, did not change significantly when the rays travelled slightly higher. On the other hand, the unrealistically high ray paths, and hence longer travel times, became more important for larger source-receiver separation distances, when no wind turbines were located closer than 3.3 km.

For comparison, the sonic gradient was calculated using the approach described in the Nord2000 model [16], which involves finding an equivalent linear sound-speed profile based on the average sound speed gradient between the source and receiver. However, it was found that the resulting sonic gradient was three times larger than the one used in this investigation and agreement between the predictions and measurements was much poorer. This is because the small associated radius of curvature resulted in ray heights that were much higher than expected, according to the results obtained using the non-linear numerical model. The approach described in the Harmonoise model [32] was also considered, however, it was found that when calculating the contribution of the wind speed gradient, the value of B_m had a negligible effect on the results. Consequently, the radius of curvature of the sound rays was governed by geometry rather than atmospheric conditions and therefore, this approach was not adopted. It is also possible that topography could influence the value of the sonic gradient that gives best agreement between the model and measurements. However, further consideration of topography is beyond the scope of this paper.

Other assumptions associated with using the model described in this investigation are that the velocity profile is constant between the source and receiver and that the profile is best described using a logarithmic fit. Although the logarithmic fit matched well with the meteorological data presented in this paper, it would not be suitable for atmospheric conditions with high refraction. Also, the velocity profile is expected to vary between the wind turbine sources and receiver, particularly due to the presence of the ridge [15]. However, to model this variation would require a much more complex approach, such as the use of the Parabolic equation, which would also require significant computa-

tional resources [15]. Further input data (such as measurements of wind profiles at multiple locations between the wind turbines and receiver locations) would also be required to adopt this approach.

The flow resistivity that was chosen in this analysis is an approximation, since this quantity was not determined from measurements. The flow resistivity can vary from 40 kPa s/m^2 for very soft ground, such as soft forest floor to 30,000 kPa s/m^2 for very hard ground, such as asphalt [27]. The correct choice of flow resistivity is dependent on the region over which the reflection of the sound wave occurs and ground surface properties may vary within this region. This is particularly true near a residence where there may be gardens, grass and asphalt all located in a relatively small area. Since the specular reflection point is expected to occur within 10 m of the residence due to the large propagation distances and large difference between the source and receiver heights, the value of flow resistivity can be difficult to predict. On the other hand, it was found that the best agreement between the model and measurements, for the frequency at which the destructive interference at a height of 1.5 m was maximum, was obtained using a realistic value of the flow resistivity for the region in which the measurements were taken. Specifically, the flow resistivity was set to 100 kPa s/m^2 for all cases, corresponding to earth and bark and sparse vegetation, which were characteristic of the surroundings of the four residences.

7. Conclusions

Although it is standard practice to measure wind farm noise at a height of 1.5 m, significant reductions in wind-induced noise can be achieved by measuring at ground level, particularly at low and infrasonic frequencies. However, the SPL measured at ground level is not equivalent to that measured at 1.5 m due to phase differences between the direct and ground-reflected ray paths. In fact, this investigation showed that the measured difference could be as high as 7 dB at the frequency corresponding to maximum destructive interference. Therefore, to allow measurements to be taken at ground level instead of 1.5 m, a microphone height correction is required.

This investigation showed that for the measurement cases considered in the analysis, which included residences located more than 2 km from the nearest wind turbine, a microphone height correction using the practical engineering model considered is not feasible. It was shown that improved agreement between the model and measurements could be achieved by taking into account the phase change due to ground reflection and incoherence due to turbulence; however, the model was still not sufficiently accurate to be used for correction purposes. Use of the plane wave reflection coefficient rather than the spherical wave reflection coefficient was found to have a negligible effect on the results, despite the significantly increased complexity associated with the latter method. Accounting for atmospheric refraction had a noticeable effect, resulting in improved agreement between the model and measurements. However, while the results from the measurements and model were within 1 dB up to 500 Hz for two of the residences, differences of 2–4 dB occurred for the other two residences at the plot minimum. These differences are a result of the inaccurate ground-reflection angles that are obtained when realistic average ray heights are used to determine the circular ray paths.

Therefore, it is recommended that outdoor measurements of wind farm noise should be taken both at ground level and at a height of 1.5 m. Measurements at ground level are advantageous at 1/3-octave frequencies below 50 Hz, where masking from wind-induced noise is most significant. At these frequencies, the wind farm noise component is equivalent at ground level and at a height of 1.5 m; however, the signal-to-noise ratio is significantly increased for the ground-mounted microphone. At 1/3-octave frequencies greater than 50 Hz, results measured at 1.5 m should be used.

Acknowledgements

The authors gratefully acknowledge financial support from the Australian Research Council, Projects DP120102185 and DE180100022. The authors also wish to thank the mechanical and electrical workshop staff at the University of Adelaide and the rural residents in South Australia, who assisted with this investigation.

Appendix A. Supplementary data

Supplementary data associated with this article can be found, in the online version, at https://doi.org/10.1016/j.apacoust.2019.05.015.

References

[1] Möller H, Pedersen CS. Low-frequency noise from large wind turbines. J Acoust Soc Am 2011;129(6):3727–44.
[2] Hansen K, Hansen C, Zajamšek B. Outdoor to indoor reduction of wind farm noise for rural residences. Build Environ 2015;94:764–72.
[3] Blazier Jr WE. Rc mark ii: a refined procedure for rating the noise of heating, ventilating, and air-conditioning (HVAC) systems in buildings. Noise Control Eng J 1997;45(6). 243–150.
[4] Raspet R, Webster J, Dillon K. Framework for wind noise studies. J Acoust Soc Am 2005;119(2):834–43.
[5] Morgan S, Raspet R. Low frequency wind noise contributions in measurement microphones. J Acoust Soc Am 1991;92(2):1180–3.
[6] Hansen Kristy, Zajamšek Branko, Hansen Colin. Identification of low frequency wind turbine noise using secondary windscreens of various geometries. Noise Control Eng J 2014;62(2):69–82.
[7] ANSI/ASA S12.9-7. Measurement of low-frequency noise and infrasound outdoors and in the presence of wind and indoors in occupied spaces. Technical report, ANSI; 2016..
[8] IEC 61400-11 Ed.3.0. Wind turbines – part 11: Acoustic noise measurement techniques; 2012..
[9] Hansen K, Zajamšek B, Hansen C. The influence of microphone height in the measurements of low frequency and infrasonic wind turbine noise at typical receivers. In: 23rd International Congress on Sound and Vibration. Athens, Greece; 2016.
[10] Australian Energy Market Operator. Wind farm power output data; 2015..
[11] ANSI S1.18 (R2010). Template method for ground impedance. Technical report, ANSI; 2010..
[12] Makarewicz R. Is a wind turbine a point source? J Acoust Soc Am 2011;129(2):579–81.
[13] Rudnik I. Propagation of sound in the open air, [in:] Handbook of Noise Control. New York: McGraw Hill; 1957.
[14] De Jong R, Stusnik E. Scale model studies of the effects of wind on acoustic barrier performance. Noise Control Eng J 1976;6(3):101–9.
[15] Ostashev Vladimir, Wilson D Keith. Acoustics in moving inhomogeneous media. 2nd ed. Taylor & Francis Group, LLC; 2016.
[16] Plovsing B. Comprehensive outdoor sound propagation model. Part 2: Propagation in an atmosphere with refraction. Technical Report AV1851/00, Delta; 2006..
[17] Bies DA, Hansen CH, Howard Carl. Engineering noise control: theory and practice. 5th edition. Spon Press; 2017.
[18] Stull RB. An introduction to boundary layer meteorology. Kluwer Academic Publishers; 1988.
[19] Wieringa J. Updating the davenport roughness classification. J Wind Eng Ind Aerodyn 1992;41(1):357–68.
[20] Vestas. General specification V90-3.0 MW VCRS; 2006. Available at https://report.nat.gov.tw/ReportFront/PageSystem/reportFileDownload/C09503816/002..
[21] Attenborough K. Review of ground effects on outdoor sound propagation from continuous broadband sources. Appl Acoust 1988;24(4):289–319.
[22] Attenborough K, Hayek SI, Lawther JM. Propagation of sound above a porous half-space. J Acoust Soc Am 1980;68(5):1493–501.
[23] Taherzadeh Shahram, Attenborough Keith. Deduction of ground impedance from measurements of excess attenuation spectra. J Acoust Soc Am 1999;105(3):2039–42.
[24] Abramowitz M, Stegun IA. Handbook of mathematical functions. USA: National Bureau of Standards; 1964.
[25] Plovsing B. Proposal for nordtest method: Nord 2000–prediction of outdoor sound propagation. DELTA Acoustics; 2014. Technical report.

[26] Delaney ME, Bazley EN. Acoustical properties of fibrous absorbent materials. Appl Acoust 1970;3:105–6.
[27] Hansen Colin H, Doolan Con J, Hansen Kristy L. Wind farm noise: measurement, assessment and control. 1st ed. John Wiley & Sons Ltd; 2017.
[28] Embleton Tony FW, Piercy Joe E, Olson N. Outdoor sound propagation over ground of finite impedance. J Acoust Soc Am 1976;59(2):267–77.
[29] ANSI/ASA S1.26. Methods for calculation of the absorption of sound by the atmosphere. Technical report, ANSI; 2014..
[30] Plovsing B. Comprehensive outdoor sound propagation model. part 1: Propagation in an atmosphere without significant refraction. Technical Report AV 1849/00, Delta; 2006..
[31] Salomons Erik, Van Maercke Dirk, Defrance Jérôme, de Roo Foort. The harmonoise sound propagation model. Acta Acustica united with Acustica 2011;97(1):62–74.
[32] European Commission. Common noise assessment methods in Europe (eu directive 2002/49/ec, annex ii: Assessment methods for noise indicators, annex ii–v9d-jrc2010). European Parliament; 2010. Technical report.